Enhanced Pyroelectricity Over Extended Thermal Range in Flexible Polymer Thin Films

Kaili Xie, Joulia Housseini, Pedro M Resende, Florian Le Goupil, Jean-david Isasa, Sylvie Tencé-Girault, Guillaume Fleury, Hamid Kellay, Georges Hadziioannou

Enhanced pyroelectricity over extended thermal range in flexible polymer thin films

Kaili Xie, *Joulia Housseini*, *Pedro M. Resende*, *Florian Le Goupil*, *Jean-David Isasa*, *Sylvie Tencé-Girault*, *Guillaume Fleury*, *Hamid Kellay*, *Georges Hadziioannou*

Dr. K. Xie, J. Housseini, Dr. P. M. Resende, Dr. F. Le Goupil, Dr. J.-D. Isasa, Prof. G. Fleury, Prof. G. Hadziioannou

Univ. Bordeaux, CNRS, Bordeaux INP, LCPO UMR 5629, F-33615, Pessac, France

Prof. H. Kellay

Univ. Bordeaux, CNRS, LOMA UMR 5798, F-33405 Talence, France

Dr. S. Tencé-Girault

Laboratoire PIMM, Arts et Metiers Institute of Technology, CNRS, Cnam, HESAM University, 75013 Paris, France

Dr. S. Tencé-Girault

Arkema, CERDATO, 27470 Serquigny, France

Email Address: k.xie2@uva.nl; guillaume.fleury@u-bordeaux.fr; georges.hadziioannou@u-bordeaux.fr

Keywords: *pyroelectricity, PVDF-based polymers, processing, flexible thin films, thermal/infrared detectors*

Polymer-based pyroelectric thin films are crucial functional materials at the core of flexible and lightweight electronic devices, such as wearable monitoring sensors, energy harvesters, and infrared detectors. Nevertheless, the pyroelectric properties of the polymer films, such as poly(vinylidene fluoride-trifluoroethylene) (P(VDF-TrFE)), vanish when the surrounding temperature exceeds the ferroelectric-to-paraelectric transition temperature, and thus limits their pyroelectric performance to a low-temperature range. Herein, we propose to mitigate this issue by employing a new class of P(VDF-TrFE) copolymer which has a low TrFE molar content. Fine tuning of the structure through thermal annealing in a vacuum environment significantly favors robust and highly polarized polymer films with a large area. Electric poling combined with an optimal annealing temperature (110-120 °C) gives highly ordered ferroelectric crystalline domains in the polymer films. Consequently, this remarkably broadens the temperature range (roughly up to 140 °C) for which the polymer film still presents high pyroelectric properties (pyroelectric coefficient 50 μC/(m^{2}K)). This study provides an alternative choice for pyroelectric polymer films with enhanced pyroelectricity in applications that require wider temperature ranges.

1 Introduction

Thin films of pyroelectric polymers such as poly(vinylidene fluoride) (PVDF) and its copolymers [1, 2] and terpolymers [3–5] have attracted much attention due to their flexibility, printability, and cost-effectiveness in contrast to inorganic ceramics like lead zirconate titanate (PZT) and barium titanate (BaTiO3) [6]. They are widely used in energy harvesting [7–10], electric sensors [11–13], and hold great promise in the manufacturing of lightweight, flexible, and wearable electronic devices. One striking example is infrared

imaging using pyroelectric polymer detector arrays, which can be prepared inexpensively by printing very thin layers of polymer over a large area [14, 15]. Unlike photoelectric detectors, the detectivity of PVDF-based polymer thermal/infrared detectors does not depend on the wavelength of the incident radiation, as long as the radiation is absorbed and converted to electric signals [16, 17]. However, the conversion efficiency from heat to electricity in PVDF-based polymer detectors often remains relatively low, resulting in poor signal to noise ratio. Furthermore, the low transition temperature from the ferroelectric to paraelectric phases in the PVDF-based polymer films often limits the applicable temperature of infrared detectors [18, 19] to low values, particularly in cooling-free applications. These constraints significantly restrict the performance of the detectors.

At the macromolecular level, the pyroelectric properties of PVDF-based polymers originate from the strong dipole due to the difference in electronegativity of the hydrogen and the fluorine atoms across the backbone [6]. There are several crystalline phases that have been proposed for the semi-crystalline PVDF polymers [6, 20, 21]. The non-polar α phase with *TGTG'* chain conformation is the most thermally stable phase in PVDF polymer. In contrast, the polar β phase, characterized by an all-*trans* ($TTTT$) planar-zigzag chain conformation, is the primary phase that imparts permanent dipoles contributing to the ferroelectricity of the polymer [22]. Chemically introducing a co-monomer, such as trifluoroethylene (TrFE), with certain molar ratios into PVDF polymer can result in a shift in polymer crystallization that favors a more highly polar β phase due to asymmetric stretching on the chain backbone [23]. Nevertheless, the polar β phase undergoes a ferroelectric-to-paraelectric transition when the temperature exceeds a critical value (Curie temperature). This phase transition temperature is highly dependent on the TrFE content [24, 25] and can therefore be tuned, ranging from 50 °C for P(VDF-TrFE) 50/50 to 135 °C for P(VDF-TrFE) 80/20 molar ratios [26–29]. However, adding less TrFE may lead to a reduction in the pyroelectric properties of the polymer film [26]. The challenge lies in determining how to enhance the pyroelectric properties of the P(VDF-TrFE) copolymer while expanding the temperature range over which pyroelectricity is sustained through proper processing treatments.

There are various processing approaches that have been suggested to improve the pyroelectric properties of PVDF-based polymer thin films, including the use of solvents with high dipole moment [30–32], purifying the polymer using solvent extraction [27], thermal annealing under optimized temperature conditions [1, 4], and electric poling over the coercive field [33]. Among these, thermal annealing and electric poling are considered as the most effective processes for modifying the crystalline structure of polymer films, and consequently, enhancing their pyroelectric performance. Thermal annealing provides polymer chains with the mobility required for crystalline lamellae thickening, thereby altering the crystalline structure and size. Meanwhile, electric poling enables the alignment of the dipoles in the crystalline domains that lead to polarization in the films (Figure 1a). Heating the polymer film during electric poling

has been shown to enhance the pyroelectric coefficient [34, 35]. However, early electric breakdown [36] during the electric polarization often occurs thus limiting device reliability. The polarization failure is attributed to the presence of impurities and/or air bubbles, even in minute quantities, in the polymer films, thus making the poling of large area films more challenging [14, 37]. Navid *et al.* [27] purified the polymer solution using solvent extraction to reduce the effect of impurities and obtained a higher polarization compared to the control experiment, resulting in a pyroelectric coefficient of 50.9 μC/(m^{2}K) and a dielectric constant of 19.4 at 1 kHz; however, the purification process is complicated and time-consuming. California *et al.* [38] studied the effect of solvent evaporation rate on the preparation of polymer thin films and concluded that a high evaporation rate does not necessarily lead to improved crystalline properties; however, it might result in low porosity in the films, which is beneficial for reducing electric breakdown [36]. Spampinato *et al.* [1] reduced the annealing time from a few hours to tens of minutes at an optimal temperature, consequently achieving a remanent polarization of 8.9 μC/cm^2; yet, the pyroelectric coefficient is not reported. Despite extensive efforts to enhance pyroelectricity, most of the focus has been on the P(VDF-TrFE) copolymers with a low Curie transition temperature ($T_c < 110$ °C). To our knowledge, pyroelectric polymers with a higher ferroelectric-to-paraelectric transition temperature have not been reported. The extent to which processing, such as annealing conditions and polarization, in the preparation of pyroelectric sensors or detectors alters and extends the phase transition temperature while enhancing pyroelectricity remains unknown.

In this work, we report and explicitly characterize a pyroelectric copolymer with a lower molar content of TrFE in a P(VDF-TrFE) copolymer, wherein the ferroelectric-to-paraelectric transition temperature can be extended close to the melting regime through optimized processing. The copolymer films are annealed in vacuum to promote the thickening and densification of the crystalline lamellae. Robust and highly polarized polymer films with a large area are achieved by simple electric poling at room temperature. The polymer film can maintain high pyroelectric features and low dielectric loss up to the melting temperature (approximately 140 °C). This significant extension broadens the applicable temperature range of the polymer for various applications. A combination of various characterizations allows the monitoring of the evolution of the degree of crystallinity, the ferroelectric phase content, and the dielectric properties of the copolymer, and reveals that simply combining thermal annealing in vacuum and electric poling at room temperature can result in an excellent pyroelectric performance of the detector. We also develop a straightforward measurement set-up to determine the response to thermal variation for the detector. Our study offers an alternative choice of P(VDF-TrFE) copolymers for the design of thermal/infrared detectors that require a wide applicable temperature range.

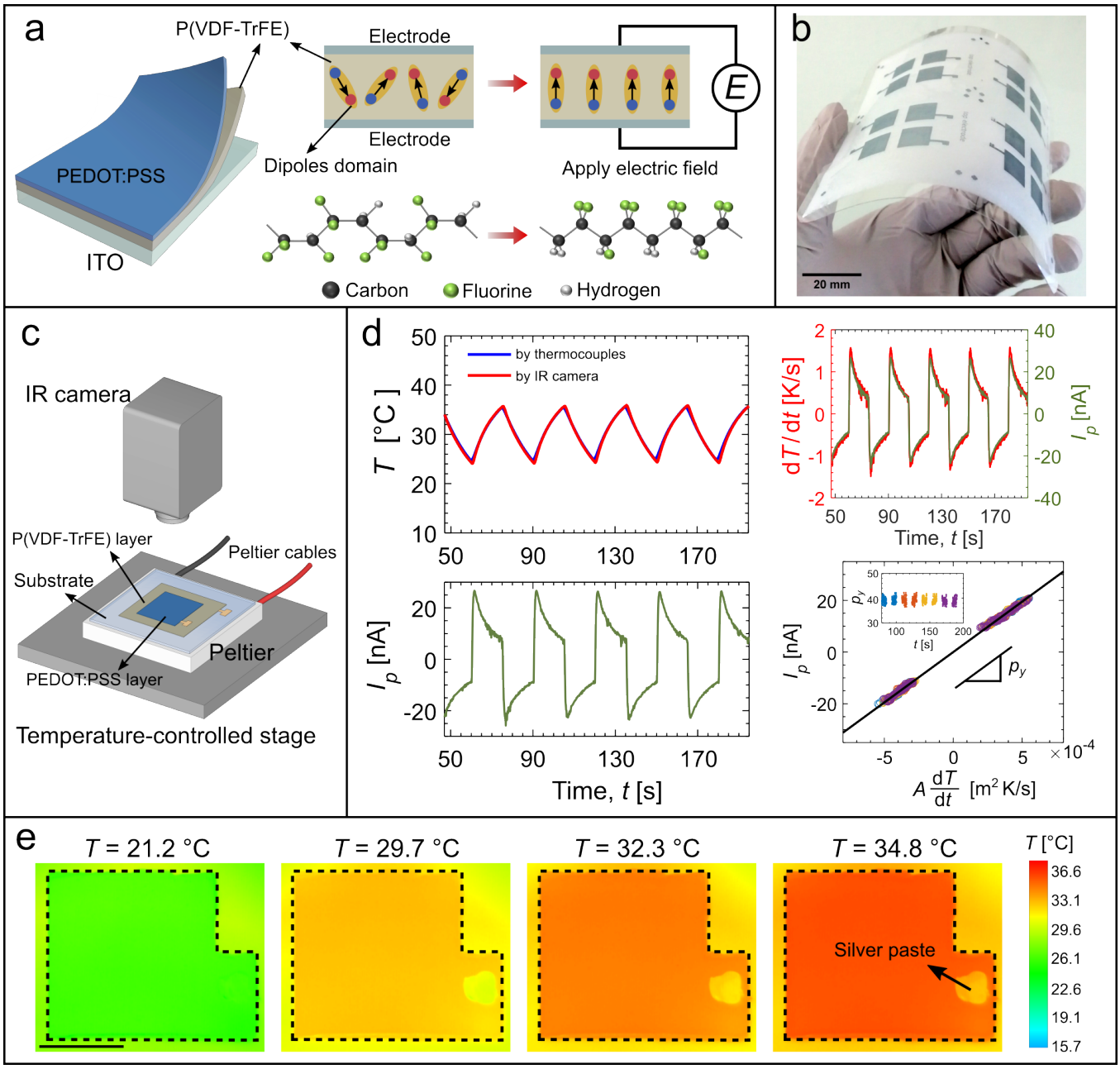

Figure 1: **Pyroelectric devices and pyroelectricity measurement. a**, Schematic of a sandwich-structured device and the electric poling process. The dipoles are aligned along the direction of the electric field when a voltage higher than the coercive field is applied. This converts the non-polar α phase into the polar β phase. **b**, An example of a flexible sensor array prepared fully by printing. **c**, Experimental setup for pyroelectric coefficient measurement. The input thermal signal is well controlled by a Peltier and a temperature-controlled stage. The temperature is measured by thermocouples and an infrared camera. Spontaneous pyroelectric current is measured by a semiconductor analyzer. **d**, Temperature and pyroelectric current. The contactless measurement of temperature using the infrared camera yields consistent results with the thermocouples and allows to check for the homogeneity of the temperature across the sample area. The pyroelectric current I_p exhibits no phase lag with respect to the temperature change rate dT/dt over time. The pyroelectric coefficient can be measured by the slope of I_p versus $A\frac{dT}{dt}$, where A is the surface area. **e**, Thermal images captured by the infrared camera. A homogeneous temperature field is observed across the large area device (roughly 2 cm × 2 cm). Dashed frames indicate the boundary of PEDOT:PSS electrode. The bright spot corresponds to the silver paste (different colors due to the different emissivity). Scale bar: 10 mm.

2 Results and discussion

2.1 Thin film preparation and pyroelectricity characterization

A thin active pyroelectric layer of P(VDF-TrFE) copolymer, with a proportion of 83% VDF and 17% TrFE (confirmed by NMR, Figure S1, Supporting Information), was deposited onto an ITO-coated glass or an ITO-coated flexible polyethylene terephthalate (PET) substrate by using a Doctor Blade technique [39, 40] or screen printing [41] (Experimental section, Figure S2 in Supporting Information). The processing conditions of P(VDF-TrFE) films are known to significantly influence the formation and nature of the crystallites within the polymer, thus determining the final pyroelectric performance of the device [4, 30, 36]. Post thermal annealing is one of the essential steps in processing. Proper annealing treatment can modify the morphology of the P(VDF-TrFE) layer, changing it from a smooth surface to rod-like grains (Figure S3, Supporting Information), often leading to enhanced ferroelectric properties. Here, contrary to the traditional annealing approach [1, 2, 30], we initially pre-dried the P(VDF-TrFE) liquid film in a vacuum chamber at room temperature for 20 minutes. This process eliminates the air bubbles trapped within the liquid films and reduces potential defects [36]. The film was then dried and annealed in a vacuum oven, with the temperature pre-set to the desired value (Figure S2, Supporting Information). The films annealed under vacuum exhibit rod-like crystalline structures compared to those annealed under ambient pressure (Figure S3, Supporting Information). A layer of conductive polymer ink poly(3,4-ethylenedioxythiophene) poly(styrenesulfonate) (PEDOT:PSS) was thereafter printed on top of the P(VDF-TrFE) layer as the top electrode (Figure 1a,b and Figure S2). Scanning electron microscopy (SEM) images confirmed the sandwich-like structure of the device (Figure S4, Supporting Information).

To determine the pyroelectricity of the P(VDF-TrFE) polymer layer, the capacitor-like device was periodically heated and cooled using a home-made setup, consisting of a Peltier and a cooling block (Figure 1c, Figure S5 in Supporting Information). The temperature of the device was measured both by thermocouples that adhered to the device and a contactless approach using an infrared camera [13]. The pyroelectric current generated was measured spontaneously in short-circuit conditions using a semiconductor device analyzer with a current resolution of picoamperes (pA). In contrast to the charge measurement for determining pyroelectricity [42], our current measurement approach is faster and significantly less susceptible to drift. The pyroelectric coefficient can be directly obtained from the measurements of the temperature and the current (Figure 1d, details in Experimental Section). Infrared images (Figure 1e) confirm the temperature homogeneity of the device during both heating and cooling phases. The uniform temperature field therefore rules out the presence of mechanical stresses that result from temperature gradients within the polymer film [14]. Furthermore, the P(VDF-TrFE) layer has a small thickness, approximately 10-20 μm, allowing the temperature field to rapidly reach equilibrium in the direction

along thickness. Consequently, the secondary pyroelectric coefficient induced by thermal stress gradients was considered negligible [42].

The pyroelectric current precisely synchronizes with the rate of temperature change (the derivative of temperature, dT/dt, with respect to time t) rather than the temperature itself (Figure 1d). The maximum rate of change of the temperature dT/dt is around 2 K/s (peak value) in our measurements, mainly due to the limitation of the power of the Peltier element used. However, this temperature rate is sufficiently high to yield a pyroelectric current well above the noise level (typically over 30 nA). This current is proportional to the rate of change of the temperature, dT/dt, as predicted by $I_p = p_y A \frac{dT}{dt}$ (see details in Supporting Information). The slope of the variation of the pyroelectric current versus the temperature rate of change therefore yields the averaged pyroelectric coefficient, p_y, with a known surface area A. Further, the instantaneous values of p_y as depicted in the inset in the bottom-right of Figure 1d are consistent with the average value of the pyroelectric coefficient. When switching between heating and cooling cycles, the device changes the direction of the pyroelectric current. This phenomenon arises from the need for the charges on the two electrodes to compensate for the change in dipole moment within the P(VDF-TrFE) layer [7] (Figure S6 in the Supporting Information). During heating, the dipole moment decreases, and the polymer volume expands, resulting in a lower polarization density. Consequently, current flows through the external circuit to balance the charge density. Conversely, when the device cools down, it induces a higher polarization density, leading to a reversed current flow.

2.2 Intrinsic properties of the copolymer

A ferroelectric material generally undergoes a phase transition from ferroelectric to paraelectric when the temperature increases. Above the transition, the crystalline structure becomes centrosymmetric with a zero net dipole moment. Ferroelectric materials depolarize above the Curie temperature, T_c. This is one of the important parameters that determines the performance of a ferroelectric material. A higher Curie temperature is desirable to achieve improved thermal stability and a broader temperature range for applications. To determine the Curie temperature of the P(VDF-TrFE) copolymer, we first performed a differential scanning calorimetry (DSC) measurements on the polymer powder in the temperature range between -50 °C and 200 °C with a rate of 10 °C/min. As shown in Figure 2a, in the first heating, we only observed an endotherm in the heat flow which corresponds to a solid to liquid phase transition at the melting temperature T_m. In the cooling process, the first exotherm corresponds to the solidification of P(VDF-TrFE) polymer while the second exotherm is attibuted to the Curie temperature where the polymer shifts from the paraelectric to the ferroelectric phase. This thermal hysteresis is typical of ferroelectrics and has previously been observed for other ratios of P(VDF-TrFE) copolymers [43]. The second

heating shows similar result as the first heating ramp giving the melting temperature T_m = 146 °C for this P(VDF-TrFE) 83/17 copolymer. Note that there is no Curie transition observed for this polymer in the heating process, which shows a remarkable difference from other ratios of P(VDF-TrFE) polymers [1]. One hypothesis is that the Curie temperature of P(VDF-TrFE) 83/17 copolymer is within the melting regime. The transition to the paraelectric phase thus occurs during the polymer melting process.

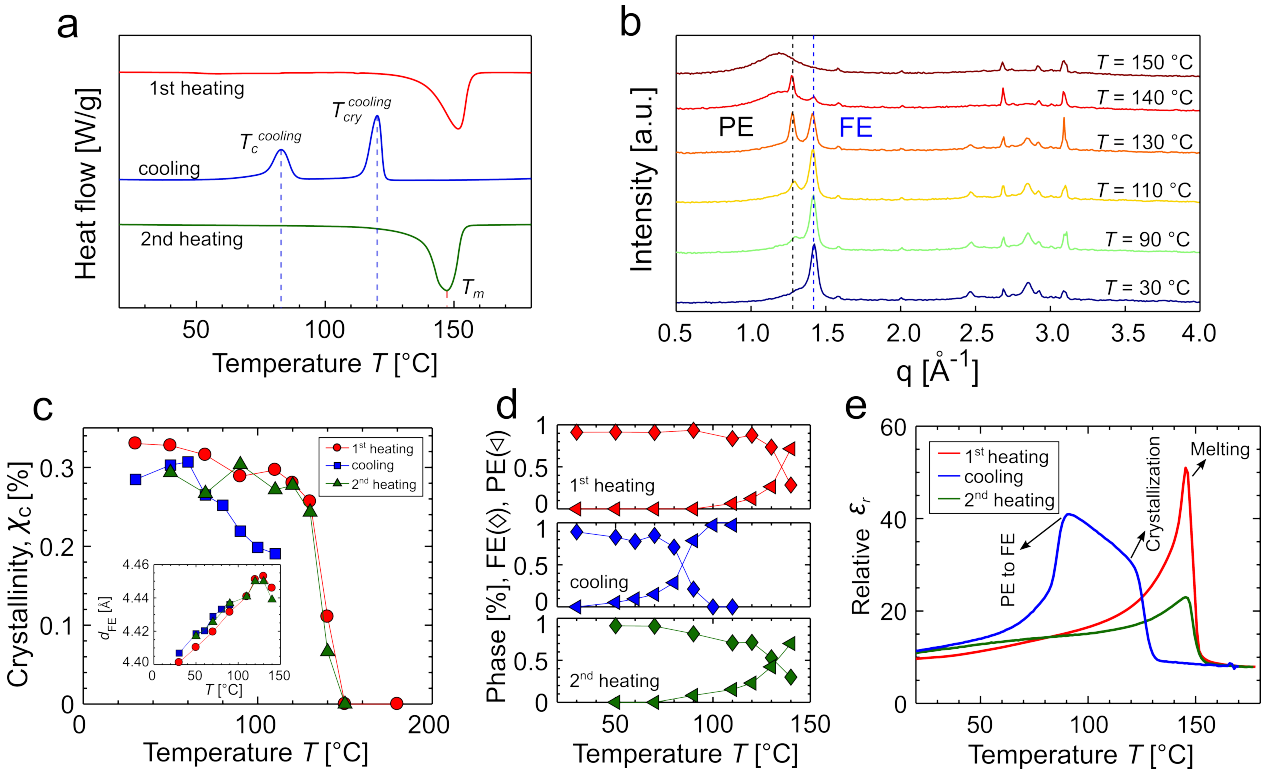

Figure 2: **Characterizations of the pyroelectric polymer. a**, DSC measurements of the polymer as received. The measurement was performed at a temperature rate of 10 K/min. The differential heat flow was normalized to the sample weight. **b**, *In-situ* WAXS measurements at different measuring temperatures. The data shown here is based on the second heating which will erase any effects of processing in the film preparation. The film was prepared using an annealing temperature 110 °C for 60 minutes in vacuum. **c**, The crystallinity degree *versus* the measuring temperatures from the WAXS data. Inset: interplanar distance of the ferroelectric phase. **d**, The fractions of ferrorelectric (FE) and paraelectric (PE) phases with the measuring temperatures in the heating and cooling processes. **e**, Relative permittivity measured by a temperature sweep (fixed frequency of 1 kHz, at 5 K/min).

The position of the Curie transition was further characterized by *in-situ* Wide-Angle X-ray Scattering (WAXS) measurements on the unpolarized P(VDF-TrFE) film at various temperatures ranging from 30 °C to 180 °C (see details in Supporting Information). A single peak was observed at low temperatures located at the wave vector q = 1.418 Å^{-1} (a diffraction angle 2θ = 20.03°) corresponding to the FE phase with dense β phase (all-*trans*), as shown in Figure 2b. However, when the temperature is increased, a second peak with q = 1.275 Å^{-1} (2θ = 18°) appears, which is associated with the PE phase. At T = 130 °C, both phases coexist. Above T = 140 °C, the PE phase becomes dominant, and the peak

shifts to a slightly lower q = 1.176 Å^{-1} at T = 150 °C. The temperature scanning in the *in-situ* WAXS measurement reveals that the FE-to-PE phase transition is situated approximately at $T_c \approx 140$ °C. Indeed, PVDF homopolymer [44] has been reported to show no FE-to-PE transition before the melting point ($T_m \approx 180$°C). This confirms our hypothesis that the Curie temperature is within the melting regime, as observed in the DSC measurement, and it is consistent with previous reports [24, 25] on low molar content of TrFE increasing the Curie temperature.

We further tracked the crystallinity degree and the proportions of the FE and PE phases in the P(VDF-TrFE) polymer film at different temperatures (Figure 2c,d). The crystallinity exhibits a dramatic decrease at 140 °C in both the first and second heating processes. This also coincides well with the results in Figure 2b and Figure 2d. At a higher temperature (150 °C), the crystallinity degree drops to zero, indicating that the film has completely melted. The cooling ramp in WAXS data also confirms our observations in DSC measurement: the polymer crystallizes at a temperature around 120 °C and exhibits more ferroelectric features when the temperature is below 85 °C. The inset of Figure 2c shows the temperature dependence of the interplanar distance of the ferroelectric phase. The interchain spacing of the polymer crystalline phase [45] exhibits a linear correlation with temperature when it is below 130 °C but experiences a sudden decrease thereafter. This is because the polymer enters the melting regime (Figure 2a). DSC and WAXS data show that the Curie temperature and the melting temperature of the P(VDF-TrFE) 83/17 copolymer are closely aligned, indicating the coexistence of the FE to PE phase transition with the melting process.

An alternative method to determine the copolymer phase transition is by measuring the temperature-dependent relative permittivity (see Experimental Section). As shown in Figure 2e, upon heating, the relative permittivity ε_r only exhibits a slight increase when the temperature is below 120 °C. However, it increases rapidly when the temperature exceeds 130 °C, at which point it enters the phase transition and melting regime of the polymer. Upon cooling, the permittivity ε_r first increases and then decreases dramatically, in accordance with the DSC thermographs, corresponding to the crystallization and paraelectric to ferroelectric transition, respectively. The polymer film also maintains a low value in dielectric loss up to near the melting temperature (Figure S7). In summary, compared to other molar ratios of VDF-based copolymers and terpolymers [2, 4, 45, 46], this P(VDF-TrFE) copolymer is expected to provide a broader operating temperature range while maintaining good pyroelectric properties for various applications such as infrared detectors and thermal imaging [16, 18, 47].

2.3 Effect of processing on the pyroelectricity

A crystalline ferroelectric material consists of crystallites that can form ferroelectric domains with a specific polarization axis. However, the random orientations of these domains results in the material exhibiting non-polar macroscopic properties. Electric poling favors the alignment of crystal domains to achieve polarization in the material, resulting in an increase in overall crystallinity and pyroelectricity [9, 24]. Figure 3 compares the WAXS patterns of FE and PE phases in the unpolarized and polarized polymer films measured at various temperatures. Below 130 °C, the FE phase is notably dominant in both the unpolarized and polarized polymer films (Figure 3a,b). With increasing temperature, the ferroelectric features in the unpolarized film decrease and completely disappear for temperatures above 140 °C (Figure 3a). However, the polarized polymer film maintain the ferroelectric features up to the melting point of the polymer. The PE phase remains negligible in contrast to the FE phase even at the temperature of 140 °C (Figure 3b). Compared to the ferroelectric content at $T = 30$ °C, there is only a 15% decrease for the polarized film, while a reduction of 60% is observed for unpolarized films (Figure 3c). The electric poling can shift the Curie temperature towards an even higher value (greater than 140 °C), further widening the applicable temperature range of the polymer films.

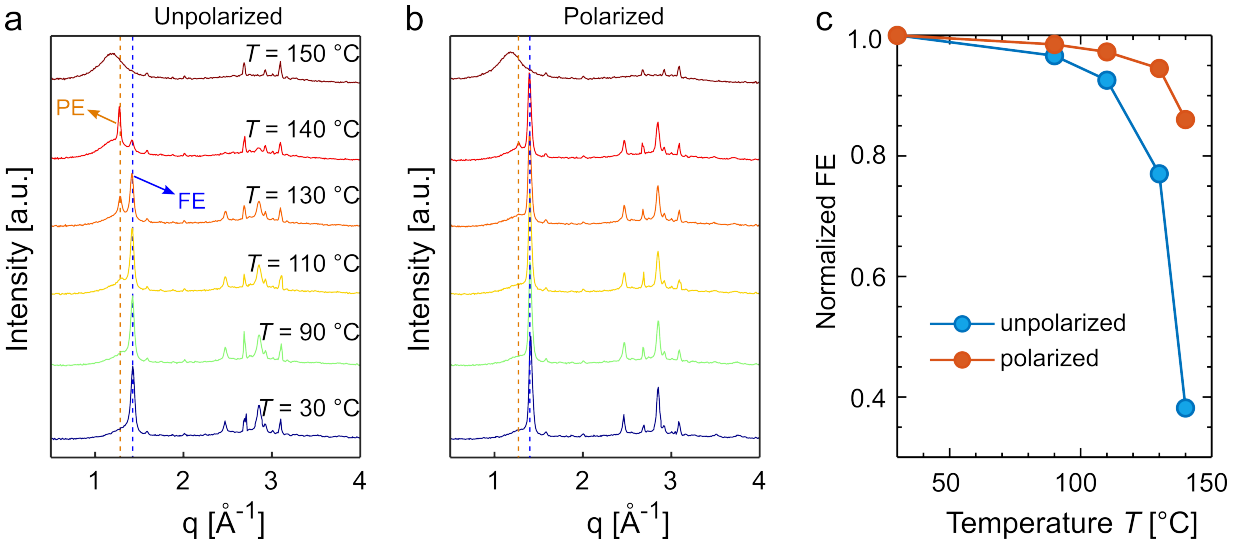

Figure 3: ***In-situ* WAXS measurement at different measuring temperatures. a**, Polymer film without electric poling. **b**, Polymer film after electric poling. **c**, Normalized intensity of ferroelectic phase (FE) with respect to the temperature of $T = 30$ °C in both unpolarized and polarized films. The films were prepared at 110 °C for 60 min with similar thickness of 20 μm. The polarized film has a remanent polarization of 8.7 μC/cm^2 and a coercive field of 50 MV/m (see Supporting Information for further details).

The ferroelectric polarization is bi-stable. When the direction of the electric field is reversed, it leads to an inversion of the dipole orientation. This gives rise to a typical ferroelectric hysteresis loop (Figure 4a). The curve shape of the polarization *versus* electric field (P-E) is remarkably influenced by the pro-

cessing during the preparation of pyroelectric devices, *e.g.*, the thermal annealing conditions [1, 2, 25]. Figure 4a compares the P-E loops of the polymer films prepared under various annealing temperatures (ranging from 70 to 150 °C) for a fixed duration of 60 minutes in a vacuum oven (see details in Experimental Section). FT-IR spectroscopy was applied to ensure that all the films were completely dried after the annealing process. Increasing the annealing temperature shifts the S-like shape of the P-E loop towards a square-like shape. The remanent polarization P_r (residual spontaneous polarization at zero electric field) is found to increase as the annealing temperature T_a increases from 70 °C to 110 °C (Figure S8 in the Supporting Information). A slight decrease in remanent polarization is observed if the annealing temperature exceeds 120 °C. The maximum value of P_r (approximately 8.6 μC/cm^2) is achieved at the annealing temperature of 110-120 °C, where the coercive field E_c (electric field where the polarization drops to zero upon field reversal) also reaches its minimum value (see inset in Figure S8). The larger remanent polarization and lower coercive field give rise to better pyroelectric performance in response to the surrounding temperature change (discussed later in Figure 4f).

Figure 4b depicts the pyroelectric coefficient p_y of the devices prepared under various annealing temperatures T_a. Thermally annealing the polymer film at 120 °C increases the pyroelectric coefficient threefold compared to 70 °C. A further increase in the annealing temperature ($T_a > 120$ °C) proves detrimental and induces a slight decrease in p_y values. This agrees well with the changes in remanent polarization with the annealing temperature (Figure S8). Annealing duration of 15 minutes and 60 minutes, as used in this work, yield similar results. This indicates that using the vacuum thermal annealing process can significantly reduce the required annealing duration, instead of taking several hours in the traditional annealing [2, 48]. This short time annealing is particularly interesting for industrial applications where time-consuming and energy-consuming processes are not desirable.

To understand how the annealing temperature sets the pyroelectric coefficient, we further conducted DSC and WAXS measurements. As shown in Figure 4c, thermal annealing treatment favors high crystallinity within the polymer film. The crystallinity degree reaches its maximum value ($\approx 46\%$) at the annealing temperature of 110 °C and 120 °C, at which the ferroelectric phase content is also maximized (Figure 4c, inset). This trend, which was also verified by DSC, shows that an optimal thermal annealing leads to a better formation of the ferroelectric crystalline phase. Additional Raman spectroscopy [49] further sheds light on the polymer chain conformation and evolution with the annealing temperature (Figure S9, Supporting Information). The intensities of the Raman bands at 266 and 1288 cm^{-1}, corresponding to the ferroelectric β phase, increase with the annealing temperature, and reach maxima at around 110 °C (Figure 4d). A similar behavior was observed using FT-IR spectroscopy (Figure S10 in Supporting Information), with the highest intensity for the β phase associated modes (840 and 1283 cm^{-1}) being detected for an annealing temperature of around 110 °C. These measurements in combination with

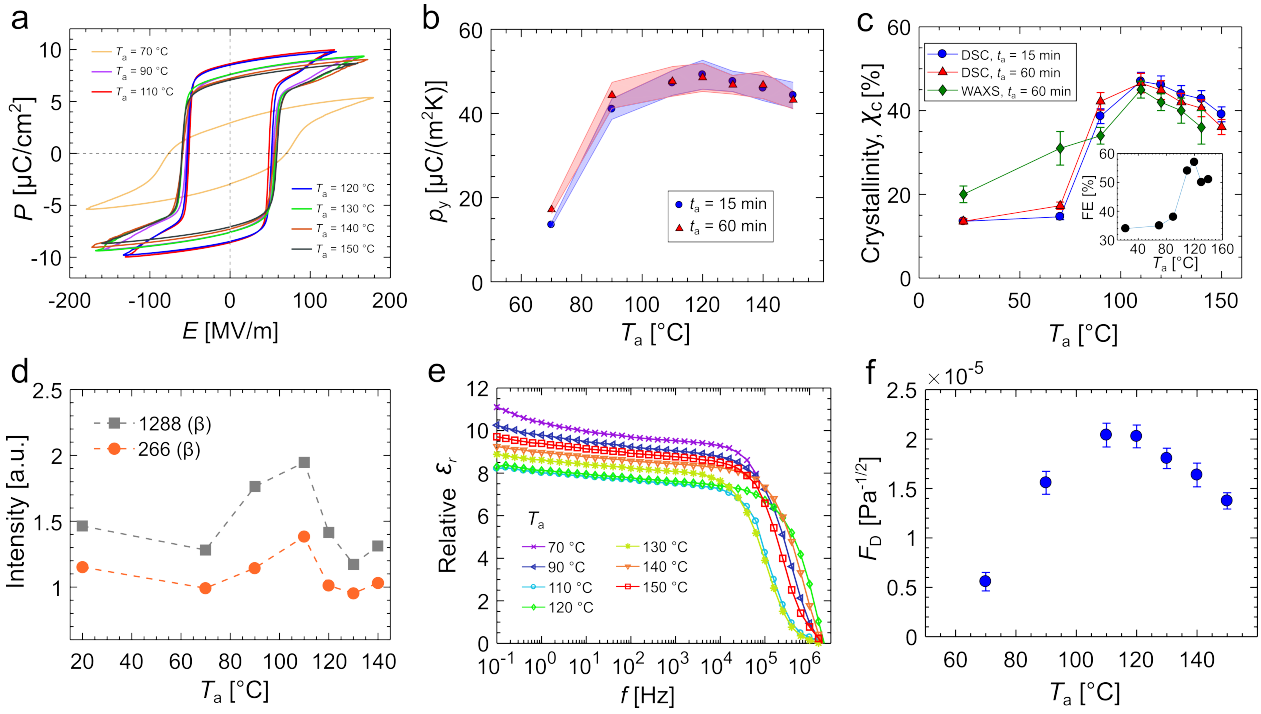

Figure 4: **Pyroelectricity under various processing**. **a**, Polarization-electric field (P-E) hysteresis loops. The P(VDF-TrFE) layers in the devices were annealed at different annealing temperatures T_a for 60 minutes, then polarized using a triangular electric field. **b**, Pyroelectric coefficients at different annealing temperatures. Two annealing durations (15 min and 60 min) were applied. The shade indicates the standard deviation from 3-5 different measurements. **c**, Crystallinity degree *versus* annealing temperature. The data were obtained from the first heating process in WAXS and DSC. Inset illustrates the fraction of FE phase variation with the annealing temperature. **d**, Raman analysis shows the β phase (corresponding to FE) in the films with different annealing temperatures. **e**, Evolution of the relative dielectric permitivitty for films electrically poled. **f**, Detectivity of the device prepared under different annealing temperatures. All the measurements were performed at room temperature except the DSC measurement in c.

WAXS and DSC data confirm that the polymer films annealed at 110-120 °C present the highest content of the electroactive phase and the highest crystallinity, but with a low occurrence of defects (such as *TTTG* or *TG* defects). This processing is thus believed to give rise to the best pyroelectricity of the device.

Figure 4e depicts the dielectric properties of the polarized polymer films prepared under different annealing temperatures. The relative permittivity ε_r presents only a slight decrease with frequency, up to 10^4 Hz. Beyond this point, it decreases dramatically as expected for dipolar polarization. The relative permittivity also decreases with the annealing temperature until reaching the values of 110 °C and 120 °C, corresponding to the optimum pyroelectricity as discussed above. This result arises from the stabilization of the dense ferroelectric phase, in which the dipoles are typically less mobile than in gauche-rich phases, and thus shows a lower dielectric permittivity for a given value of crystallinity. Temperatures higher than 130 °C result in a shift of ε_r towards larger values. The dielectric loss remains at relatively

low values, fluctuating between 0.015 and 0.025, and reaching its minimum value for an annealing temperature of 110 °C.

To evaluate the pyroelectric performance of our devices, we employ the figure of merit (FoM) defined as $F_D = p_y/(c_v\sqrt{\varepsilon_0\varepsilon_r \tan\delta})$, where c_v is the volumetric specific heat [50], ε_0 refers to the vacuum permittivity, and $\tan\delta$ is the dielectric loss. This FoM sets the detection capability, which is expected to be optimized by maximizing the pyroelectric coefficient and minimizing the dielectric loss for a given material. Figure 4f shows the evolution of the detectivity F_D with the annealing temperatures. In accordance with our results discussed above, our pyroelectric detector annealed at the optimum temperature results in the best pyroelectric sensitivity. Optimal processing can increase the detectivity 4-fold compared to annealing at low temperatures (such as $T_a = 70$ °C). This is mainly because optimal annealing results in a high pyroelectric coefficient while maintaining low permittivity and dielectric loss (Figure 4b,e). Regarding the detectivity of the pyroelectric detector, our strategy utilizing P(VDF-TrFE) 83/17 copolymer with optimal processing can yield values 1.5-3 times higher than those reported for P(VDF-TrFE) 50/50, 70/30, and 80/20 copolymers in the literature [51, 52], and can be even 4 times higher compared to the copolymer doped with a ceramic material (such as Pz59) [14].

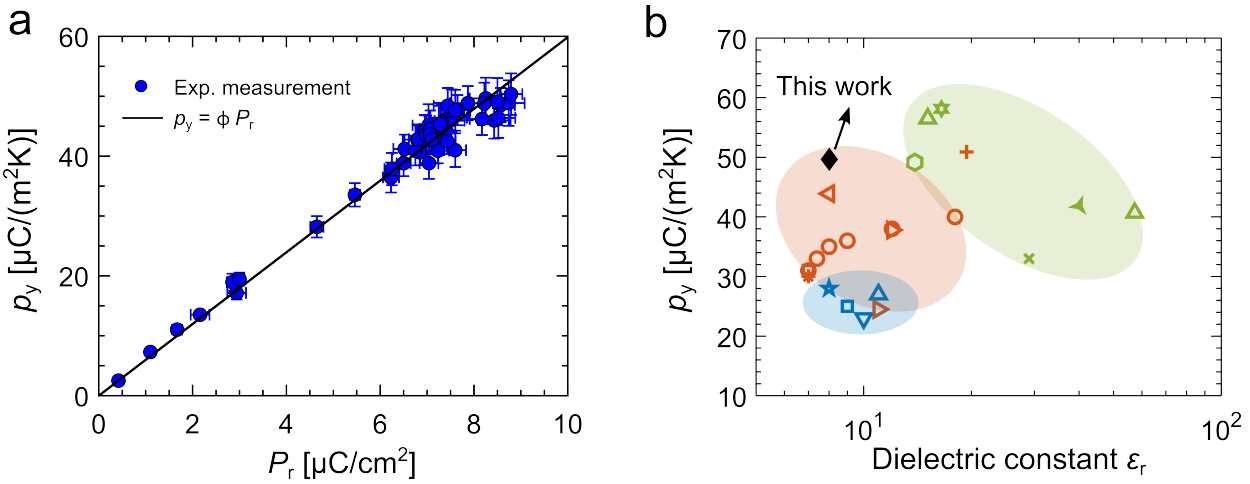

Figure 5: **Pyroelectricity. a**, Pyroelectric coefficient as a function of remanent polarization, measured at room temperature. **b**, Map in the parameter space of p_y and ε_r. Blue region: PVDF; Orange: P(VDF-TrFE); Green region: doped-P(VDF-TrFE). Different symbols indicate different references in literature [2, 14, 19, 26, 27, 30, 35, 44, 53–57], summarized in Table S1 in Supporting Information.

Figure 4b and Figure S8 show a similar trend in the pyroelectric coefficient p_y and the remanent polarization P_r with respect to the annealing temperature. To explore this, we performed the pyroelectric measurements for devices with varying remanent polarization. Note that we utilized devices prepared with different annealing temperatures and various polarization degrees. As illustrated in Figure 5a, the pyroelectric coefficient aligns well with the linear prediction, $p_y = \phi P_r$, where ϕ represents a con-

stant factor. The constant factor might be influenced by the material itself as well as the processing. In our measurements, the constant $\phi \approx 6\times10^{-4}$ K^{-1}, 6-times larger than the thermal expansion coefficient 1×10^{-4} K^{-1} reported for the PVDF-TrFE copolymer [58]. The secondary pyroelectricity contribution from the dimensional effect to the observed pyroelectric activity is not dominant. Our observation is also in accordance with a recent report [2].

Higher pyroelectric coefficients along with lower dielectric constants and dielectric losses are expected to lead to a better sensitivity for pyroelectric detectors. Here, we established a map in the space of parameters: pyroelectric coefficient p_y and relative dielectric constant ε_r, as depicted in Figure 5b. We compared the state-of-the-art VDF-based pyroelectric materials, including PVDF polymers, P(VDF-TrFE) copolymers, and P(VDF-TrFE) copolymers doped with inorganic materials (such as lead titanate (PT) powder, PNN-PZT (Pz59) powder, lanthanum and calcium modified lead titanate (PCLT), and ZnO quantum dots (ZnO QDs)), see details in the Supporting Information. In general, doping VDF-based polymers with such inorganic materials (green region in Figure 5b) allows to increase the pyroelectric coefficient, but it also induces a higher dielectric constant. Moreover, the addition of inorganic materials renders the VDF-based polymers less printable and more costly. PVDF polymer (blue region) possesses a low value in dielectric constant but also has poor pyroelectricity. In contrast, the P(VDF-TrFE) copolymers (orange region) are more attractive concerning the performance and cost-effectiveness. Our approach, using the optimized processing in preparing the pyroelectric device, can enhance the pyroelectric coefficient up to 50 $\mu C/(m^2K)$, while maintaining a relatively low dielectric constant of around 8 at room temperature.

3 Conclusion

In summary, we have thoroughly investigated the processing effects on enhancing the pyroelectric performance of a copolymer with a low amount of TrFE (P(VDF-TrFE) 83/17). We demonstrate that this copolymer can maintain excellent pyroelectric properties up to the melting temperature (up to 140 °C). This is achieved through the combination of vacuum thermal annealing and step-by-step electric poling at room temperature. We further quantitatively evaluate the effects of annealing temperatures on the pyroelectric performance of thermal detectors, showing that the optimal temperature (between 110 °C and 120 °C) can result in highly ordered ferroelectric crystalline domains within the polymer films, consequently giving a better detectivity of the pyroelectric detector. Our study provides an alternative choice of P(VDF-TrFE) copolymers for the design of thermal/infrared detectors that may require a wide applicable temperature range.

4 Experimental Section

Materials: Poly(vinylidenefluoride-*co*-trifluoroethylene) (P(VDF-TrFE)) with 83/17 VDF/TrFE molar ratio was kindly supplied by IRLYNX (France) in the form of solid pellets (≈ 3 mm in length). The average molar mass is around 233,000 g/mol. Printable silver paste (DM-SIP-3061S) was purchased from DYCOTEC Materials (UK). Conductive ink poly(3,4-ethylenedioxythiophene)-poly(styrenesulfonate) (PEDOT:PSS) (EL-P5015) used for screen printing was acquired from Agfa ORGACON. Propylene carbonate (PC) (99.5%) was received from Thermo Fisher Scientific. Acetone, ethanol, and isopropanol were purchased from Sigma-Aldrich and used as received. Deionized water was obtained from a Millipore Water filtering system (PureLab Flex). Thermal paste (7 W/(m·K)) from RS France was used. All products were used without further purification.

Polymer solution preparation: Solid P(VDF-TrFE) pellets were dissolved in PC with a concentration of 20 wt%. The choice to use PC is based on its high molecular dipole moment (4.9 D), which could potentially benefit the formation of the ferroelectric phase [30]. To dissolve the polymer, the solution was stirred using a magnetic stirrer at a temperature of 90 °C on a hot plate for two days. The heating was then turned off, and the solution was left on the hot plate to slowly cool down back to room temperature.

Substrate preparation: Flexible, indium tin oxide (ITO)-coated PET substrate (surface resistivity 100 Ω/Sq, from Sigma-Aldrich), and ITO-coated glass substrate (100 mm × 100 mm, 0.7 mm in thickness, from Guluo Glass) were used in this study. Before using, glass substrates were cleaned using acetone, ethanol, and isopropanol in an ultrasonic bath (fisherbrand, FB15062) for 15 min each and then dried with clean nitrogen gas. The PET substrates were cleaned with the same procedure, excluding the use of Acetone. Plasma treatment (10 min) was further used before the P(VDF-TrFE) layer deposition.

Film deposition, processing, and device fabrication: A rigid Doctor blade coating setup (TFC200-400) was used to deposit the polymer layer onto the pre-cleaned glass substrate (10 cm × 10 cm) or PET substrate (10 cm × 10 cm) which was fixed by the vacuum suction. A screen printer (EKRA X5) was also used to obtain thinner polymer films. The substrate was split into four areas (40 mm × 40 mm) by using Kapton tape before the P(VDF-TrFE) layer deposition. Each area formed an individual device. After deposition, the P(VDF-TrFE) liquid film was placed in a vacuum chamber for 20 min at room temperature to remove the entrapped air bubbles, followed by further drying and annealing in a vacuum oven (Medline OV-11). The dried polymer film thickness was measured using a profilometer (Bruker Dektak XT-A), roughly 10-20 μm depending on the processing. PEDOT:PSS layers were afterwards deposited onto the P(VDF-TrFE) layer as the top electrodes using a similar process, see Figure S2 in Supporting Information. The devices were stored in a glovebox under vacuum. All the fabrication, process-

ing, and measurements were performed in an ISO6 clean-room environment at ELORPrintTec (Université de Bordeaux).

Poling process: The polarization switching response to the electric field closely reflects the performance of the ferroelectric devices [59]. Electrically poling the VDF-based ferroelectric polymer at a high temperature (*e.g.*, 100 °C) might be advantageous for reducing imperfections or defects in the crystallites, thus favorably converting the α phase to the β phase [35, 60]. However, this process is complicated. In our study, the poling process was conducted at room temperature using the TF Analyzer 2000E (aixACCT Systems). A triangular wave with a frequency of 2 Hz was used. To prevent early breakdown, the voltage was increased step by step (a maximum step of 100 V), and for each step several polarization cycles were applied until the polarization-electric field (P-E) loop curves were similar. The accumulated charge [42] during the poling was discharged from the device electrodes after several steps by connecting the electrodes to the ground. For each configuration, 3-5 devices were poled, and the average P-E loop curve was obtained.

Characterizations: Differential scanning calorimetry (DSC) (Mettler TOLEDO) measurement was performed using the same rate 10 K/min in the heating and cooling processes in the temperature range between -50 °C and 200 °C. The sample was kept at 200 °C for 10 minutes to ensure complete melting. The crystallinity percentage is calculated by [30, 61] $\chi_c = \Delta H_m/\Delta H_m^0 \times 100\%$, where ΔH_m is the melting enthalpy of the polymer film, and ΔH_m^0 is the melting enthalpy of a 100% crystalline polymer. Wide-angle X-ray scattering (WAXS) measurements were performed using the Nano inXider using a transmission mode. The temperature was controlled by a Linkam HFSX350 heating plate, at a change rate of 10 K/min. Scattering patterns were collected using a Pilatus3 (Dectris) detector. It stopped 2 minutes at every temperature of interest during the pattern acquisition [62]. Fourier transform infrared (FT-IR) spectroscopy was performed using a Nicolet iS5 with an ATR module iD7 (diamond-crystal window, diameter of 1.8 mm), between 4000 to 400 cm^{-1}. Raman spectroscopy measurements were performed using an XploRa spectrometer (Horiba Instruments) coupled with an Olympus microscope. A linearly polarized laser (Nd:YAG, wavelength 532 nm) and a magnification of 50× (sampling diameter of 10 to 15 μm) were used. The measurement range was between 200 and 1600 cm^{-1}, see details in Supporting Information. The dielectric measurements were conducted in the frequency range of 0.1 Hz to 1 MHz using a Solartron 1296 dielectric system. In temperature sweep experiment, the measuring temperature was varied at a rate of 5 K/min while fixing the frequency at 1 kHz. The temperature ranged from -50 °C to 180 °C and kept at 180 °C for 10 min to ensure complete melt of the polymer before cooling down. For frequency sweep measurement, the measuring temperature was set as the room temperature. All the dielectric measurements were performed with a voltage amplitude of 1 V.

Pyroelectricity measurement: Pyroelectric coefficient was measured using a home-made setup (Figure 1c

and Figure S5). The device was fixed on a Peltier (40 mm × 40 mm, RS Pro 217-2399) using a homogeneous thin layer of thermal paste to reduce the thermal resistance. The Peltier was fixed on a temperature-controlled stage where the temperature was kept at a constant value of 14 °C. In heating, the Peltier, powered by DC power generator (Aim-TTi CPX400DP), was turned on, while in cooling the Peltier was off. The temperature of the polymer layer was measured by thermocouples (T type from Omega) and an Infrared camera (FLIR SC7000). The generated current due to the temperature change was instantaneously measured by using a semiconductor device analyzer (KEYSIGHT B1500A). A home-made Matlab program was used to synchronize the measurements of temperature and current. The average pyroelectric coefficient was therefore calculated from the continuous measurements of temperature and current over several heating-cooling periods, see details in Supporting Information.

Supporting Information

Supporting Information is available from the Wiley Online Library or from the authors.

Acknowledgements

The authors gratefully acknowledge funding from the Industrial Chair SMILE within the Grant Agreement No. ANR-19-CHIN-0002. This work was performed within the framework of the Equipex ELORPrintTec ANR-10-EQPX-28-01 with the help of the French state's Initiative d'Excellence IdEx ANR-10-IDEX-003-02. K. Xie acknowledges B. Gorin for assistance with the infrared camera, W. Smaal and S. Khiev for training in the clean room, and L. Gao for the help of schematic drawings.

Conflict of Interest

The authors have no conflicts of interest in this work.

References

[1] N. Spampinato, J. Maiz, G. Portale, M. Maglione, G. Hadziioannou, E. Pavlopoulou, *Polymer* **2018**, *149* 66.

[2] C. Ng, W. Gan, T. Velayutham, B. Goh, R. Hashim, *Physical Chemistry Chemical Physics* **2020**, *22*, 4 2414.

[3] N. Zeggai, M. Fricaudet, N. Guiblin, B. Dkhil, M. Lobue, M. Almanza, *ACS Applied Polymer Materials* **2024**.

[4] N. Pouriamanesh, F. Le Goupil, N. Stingelin, G. Hadziioannou, *ACS Macro Letters* **2022**, *11*, 4 410.

[5] F. Le Goupil, K. Kallitsis, S. Tencé-Girault, N. Pouriamanesh, C. Brochon, E. Cloutet, T. Soulestin, F. Domingue Dos Santos, N. Stingelin, G. Hadziioannou, *Advanced Functional Materials* **2021**, *31*, 1 2007043.

[6] A. Arrigoni, L. Brambilla, C. Bertarelli, G. Serra, M. Tommasini, C. Castiglioni, *RSC advances* **2020**, *10*, 62 37779.

[7] F. Gao, W. Li, X. Wang, X. Fang, M. Ma, *Nano Energy* **2016**, *22* 19.

[8] P. Lheritier, A. Torelló, T. Usui, Y. Nouchokgwe, A. Aravindhan, J. Li, U. Prah, V. Kovacova, O. Bouton, S. Hirose, et al., *Nature* **2022**, *609*, 7928 718.

[9] J. Yang, Q. Chen, F. Xu, H. Jiang, W. Liu, X. Zhang, Z. Jiang, G. Zhu, *Advanced Electronic Materials* **2020**, *6*, 10 2000578.

[10] H. Ryu, S.-W. Kim, *Small* **2021**, *17*, 9 1903469.

[11] H. Xue, Q. Yang, D. Wang, W. Luo, W. Wang, M. Lin, D. Liang, Q. Luo, *Nano Energy* **2017**, *38* 147.

[12] J. Lee, H. J. Kim, Y. J. Ko, J. Y. Baek, G. Shin, J. G. Jeon, J. H. Lee, J. H. Kim, J. H. Jung, T. J. Kang, *Nano Energy* **2022**, *97* 107178.

[13] A. Aravindhan, P. Lheritier, A. Torelló, U. Prah, Y. Nouchokgwe, A. El Moul, X. Chevalier, F. D. Dos Santos, E. Defay, V. Kovacova, *Journal of Materiomics* **2023**, *9*, 2 256.

[14] M. Dietze, M. Es-Souni, *Macromolecular Materials and Engineering* **2019**, *304*, 12 1900538.

[15] M. Fattori, S. Cardarelli, J. Fijn, P. Harpe, M. Charbonneau, D. Locatelli, S. Lombard, C. Laugier, L. Tournon, S. Jacob, et al., *Nature Electronics* **2022**, *5*, 5 289.

[16] E. S. Kulkarni, S. P. Heussler, A. V. Stier, I. Martin-Fernandez, H. Andersen, C.-T. Toh, B. Özyilmaz, *Advanced Optical Materials* **2015**, *3*, 1 34.

[17] J. Wang, H. Fang, X. Wang, X. Chen, W. Lu, W. Hu, *Small* **2017**, *13*, 35 1700894.

[18] D. Zhang, H. Wu, C. R. Bowen, Y. Yang, *Small* **2021**, *17*, 51 2103960.

[19] S. B. Lang, S. Muensit, *Applied Physics A* **2006**, *85*, 2 125.

[20] R. Hasegawa, M. Kobayashi, H. Tadokoro, *Polymer Journal* **1972**, *3*, 5 591.

[21] A. J. Lovinger, *Science* **1983**, *220*, 4602 1115.

[22] C. Park, K. Lee, M. Koo, C. Park, *Advanced Materials* **2021**, *33*, 47 2004999.

[23] A. J. Lovinger, T. Furukawa, G. Davis, M. Broadhurst, *Polymer* **1983**, *24*, 10 1225.

[24] K. Koga, H. Ohigashi, *Journal of applied physics* **1986**, *59*, 6 2142.

[25] T. Furukawa, *Advances in Colloid and Interface Science* **1997**, *71* 183.

[26] R. Köhler, N. Neumann, G. Hofmann, *Sensors and Actuators A: Physical* **1994**, *45*, 3 209.

[27] A. Navid, C. S. Lynch, L. Pilon, *Smart Materials and Structures* **2010**, *19*, 5 055006.

[28] Y. Sutani, Y. Koshiba, T. Fukushima, K. Ishida, *Polymer* **2021**, *228* 123904.

[29] R. Gregorio Jr, M. M. Botta, *Journal of Polymer Science Part B: Polymer Physics* **1998**, *36*, 3 403.

[30] J. Kim, J. H. Lee, H. Ryu, J.-H. Lee, U. Khan, H. Kim, S. S. Kwak, S.-W. Kim, *Advanced Functional Materials* **2017**, *27*, 22 1700702.

[31] G. Knotts, A. Bhaumik, K. Ghosh, S. Guha, *Applied Physics Letters* **2014**, *104*, 23.

[32] T. Wang, Y. Wang, F. Dang, M. Liu, S. Sun, K. Jin, P. Cheng, *Nanotechnology* **2023**, *35*, 7 075501.

[33] S. S. Dani, A. Tripathy, N. R. Alluri, S. Balasubramaniam, A. Ramadoss, *Materials Advances* **2022**.

[34] H. Yamazaki, J. Ohwaki, T. Yamada, T. Kitayama, *Applied Physics Letters* **1981**, *39*, 9 772.

[35] A. Aliane, M. Benwadih, B. Bouthinon, R. Coppard, F. Domingues-Dos Santos, A. Daami, *Organic Electronics* **2015**, *25* 92.

[36] Y. Zhang, B. R. Aich, S. Chang, K. Lochhead, Y. Tao, *Organic Electronics* **2022**, *105* 106494.

[37] X. Hu, M. You, N. Yi, X. Zhang, Y. Xiang, *Frontiers in Energy Research* **2021**, *9* 621540.

[38] A. California, V. F. Cardoso, C. M. Costa, V. Sencadas, G. Botelho, J. L. Gomez-Ribelles, S. Lanceros-Mendez, *European polymer journal* **2011**, *47*, 12 2442.

[39] A. Glasser, E. Cloutet, G. Hadziioannou, H. Kellay, *Chemistry of Materials* **2019**, *31*, 17 6936.

[40] K. Xie, A. Glasser, S. Shinde, Z. Zhang, J.-M. Rampnoux, A. Maali, E. Cloutet, G. Hadziioannou, H. Kellay, *Advanced Functional Materials* **2021**, *31*, 21 2009039.

[41] V. Pecunia, L. Petti, J. Andrews, R. Ollearo, G. H. Gelinck, B. Nasrollahi, J. M. Jailani, N. Li, J. H. Kim, T. N. Ng, et al., *Nano Futures* **2023**.

[42] I. Lubomirsky, O. Stafsudd, *Review of Scientific Instruments* **2012**, *82*, 5 121101.

[43] A. Pipertzis, K. Asadi, G. Floudas, *Macromolecules* **2022**, *55*, 7 2746.

[44] X. Li, S.-G. Lu, X.-Z. Chen, H. Gu, X.-s. Qian, Q. Zhang, *Journal of Materials Chemistry C* **2013**, *1*, 1 23.

[45] B. Liu, B. Tian, S. Geiger, Z. Hu, X. Zhao, Y. Zou, J. Wang, J. Sun, S. Sun, B. Dkhil, et al., *Applied Physics Letters* **2014**, *104*, 22.

[46] S. Nayak, H. T. Ng, A. Pramanick, *Applied Physics Letters* **2020**, *117*, 23.

[47] M. Shehzad, Y. Wang, *ACS omega* **2020**, *5*, 23 13712.

[48] T. Raman Venkatesan, D. Smykalla, B. Ploss, M. Wubbenhorst, R. Gerhard, *Macromolecules* **2022**, *55*, 13 5621.

[49] P. M. Resende, J.-D. Isasa, G. Hadziioannou, G. Fleury, *Macromolecules* **2023**, *56*, 23 9673.

[50] Y. Wong, N. Hui, E. Ong, H. Chan, C. Choy, *Journal of applied polymer science* **2003**, *89*, 12 3160.

[51] S. B. Lang, D. K. Das-Gupta, In *Handbook of advanced electronic and photonic materials and devices*, 1–55. Elsevier, **2001**.

[52] R. W. Whatmore, S. J. Ward, *Journal of Applied Physics* **2023**, *133*, 8.

[53] K. Tan, W. Gan, T. Velayutham, W. Abd Majid, *Smart materials and structures* **2014**, *23*, 12 125006.

[54] W. C. Gan, W. H. A. Majid, *Organic Electronics* **2015**, *26* 121.

[55] Q. Yang, Z. Shi, D. Ma, Y. He, J. Wang, *Ceramics International* **2018**, *44*, 12 14850.

[56] B. Ploss, B. Ploss, F. Shin, H. Chan, C. Choy, *IEEE transactions on dielectrics and electrical insulation* **2000**, *7*, 4 517.

[57] N. Ahmad, W. A. Majid, M. Zaini, A. Rosli, R. Adnan, N. Halim, *Materials Science and Engineering: B* **2023**, *289* 116256.

[58] T. Furukawa, *IEEE transactions on electrical insulation* **1989**, *24*, 3 375.

[59] K. Uneda, S. Horike, Y. Koshiba, K. Ishida, *polymer* **2022**, *249* 124822.

[60] R. Kepler, *Annual Review of Physical Chemistry* **1978**, *29*, 1 497.

[61] M. Gu, J. Zhang, X. Wang, W. Ma, *Journal of applied polymer science* **2006**, *102*, 4 3714.

[62] F. Le Goupil, K. Kallitsis, S. Tencé-Girault, C. Brochon, E. Cloutet, G. Fleury, G. Hadziioannou, *ACS Applied Energy Materials* **2023**, *6*, 24 12172.

Table of Contents

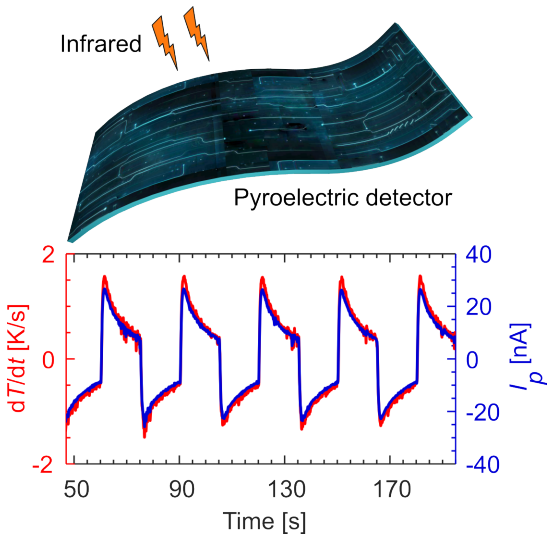

Enhanced pyroelectricity of VDF-based copolymer is achieved by largely extending the ferroelectric-to-paraelectric transition temperature. Optimized thermal annealing and electric poling processing favor highly ordered ferroelectric crystalline structures within the polymer films, resulting in a high pyroelectric features up to 140 °C. These findings sheds light on the design of high-performance flexible pyroelectric detectors.